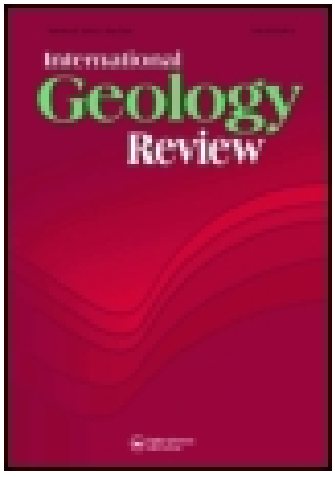

International Geology Review

Publication details, including instructions for authors and subscription information:
http://www.tandfonline.com/loi/tigr20

Mid-Miocene (~17 Ma) quartz diorite porphyry in Ciemas, West Java, Indonesia, and its geological significance

Cheng-Quan Wu[ab], Zheng-Wei Zhang[a], Chao-Fei Zheng[ab] & Jun-Hua Yao[ab]

[a] State Key Laboratory of Ore Deposit Geochemistry, Institute of Geochemistry, Chinese Academy of Sciences, Guiyang 550002, China

[b] College of Earth Science, University of Chinese Academy of Sciences, Beijing 100049, China

Published online: 29 Apr 2014.

To cite this article: Cheng-Quan Wu, Zheng-Wei Zhang, Chao-Fei Zheng & Jun-Hua Yao (2014): Mid-Miocene (~17 Ma) quartz diorite porphyry in Ciemas, West Java, Indonesia, and its geological significance, International Geology Review, DOI: 10.1080/00206814.2014.908748

To link to this article: http://dx.doi.org/10.1080/00206814.2014.908748

International Geology Review, 2014
http://dx.doi.org/10.1080/00206814.2014.908748

Taylor & Francis
Taylor & Francis Group

Mid-Miocene (~17 Ma) quartz diorite porphyry in Ciemas, West Java, Indonesia, and its geological significance

Cheng-Quan Wu[a,b], Zheng-Wei Zhang[a]*, Chao-Fei Zheng[a,b] and Jun-Hua Yao[a,b]

[a]*State Key Laboratory of Ore Deposit Geochemistry, Institute of Geochemistry, Chinese Academy of Sciences, Guiyang 550002, China;* [b]*College of Earth Science, University of Chinese Academy of Sciences, Beijing 100049, China*

(*Received 17 December 2013; accepted 24 March 2014*)

In order to constrain its petrogenesis and mineralization, a detailed study of Miocene quartz diorite porphyry from the Ciemas area of West Java, Indonesia, was undertaken, including geochronology and major and trace element analyses. Ciemas quartz diorite porphyry contains medium–coarse-grained quartz and hornblende phenocrysts in a matrix of primarily cryptocrystalline quartz and feldspar. The rocks belong to the calc-alkaline-high K calc-alkaline series. The quartz diorite porphyry and Miocene dacite and andesite wall rocks have similar compositions, both being enriched in large-ion lithophile elements (LILEs) K, Rb, Th, and U, depleted in high-field strength elements (HFSEs) Nb, Ta, Zr, Hf, and P; with light rare earth element (LREE)-enriched patterns and negative Eu anomalies, which are typical for arc magmatic rocks. LA-ICP-MS U-Pb zircon ages of andesite, amphibolic tuff breccia, and quartz diorite porphyry are 17.5 ± 0.3, 16.9 ± 0.3, and 17.1 ± 0.4 Ma, respectively. The quartz diorite porphyry formed by mid-Miocene arc magmatism. This intrusion and surrounding volcanics developed together as the Indian–Australian Plate subducted northward beneath Java, releasing fluids that triggered partial melting of the overlying mantle wedge and felsic melts that evolved further in the crust. Petrogenesis and ages of Ciemas magmatic rocks are important to gaining an understanding of Cenozoic Sunda Arc magmatism, and also provide insights into related epithermal gold deposits.

Keywords: quartz diorite porphyry; zircon U-Pb dating; arc magmatic rocks; West Java; Indonesia

1. Introduction

The Indian–Australian Plate has drifted northward since the Mesozoic and has been subducted beneath the Eurasian Plate since at least the Eocene (Katili 1975; Hamilton 1979). This subduction has resulted in magmatic activity along the convergent plate boundary, forming the Sunda–Banda Arc, which extends from the northern tip of Sumatra through Java and Bali and continues to eastern Indonesia. Java Island is a part of this arc. Java contains abundant calc-alkaline magmatic rocks which become younger from south to north (Bemmelen 1949, 1970; Katili 1975; Whitford *et al.* 1979; Nicholls *et al.* 1980; Soeria-Atmadja *et al.* 1994). These rocks have been studied in terms of petrogenesis and mineralization (Marcoux *et al.* 1994; Soeria-Atmadja *et al.* 1994).

Ciemas, located in the southwest of West Java Province (Figure 1a), has lush vegetation and rare outcrops. No research on Ciemas igneous rocks, either preliminary or detailed, has been published. In recent years, some magmatic rocks, including a quartz diorite porphyry intrusion, were exposed with the discovery of gold deposits. This intrusion is approximately 1000 m long by 500 m wide, intruding dacite and andesite (Figure 1). The petrogenesis and age of the intrusion and wall rocks have not been reported to date. We sampled both the porphyry and wall rocks and studied the petrogenesis and ages of the rocks using zircon U-Pb dating methods and whole-rock major and trace elements. In addition, some epithermal gold veins, such as Cibak, Cikanteh, and Cileuweung (Figure 1(b)), were found near the intrusion. The study of petrogenesis and ages of the intrusion and wall rocks is useful to gaining an understanding of the genesis of the gold veins.

2. Geological background

Ciemas is located 100 km south of Jakarta in southwestern Sukabumi County (Figure 1(a)). Geologically, it lies near the convergence zone of the Indian–Australian and Eurasian Plates.

Major sedimentary strata in the study area include: (1) the Jampang Formation, comprising fine- to coarse-grained pyroclastic rocks composed of phyric augite andesite, hornblende andesite, dacite, and porphyritic basalt rubble clastics interbedded with lava, tuff, and coral limestone; (2) the Cikarang Layer of the Jampang Formation, which primarily consists of volcanic tuff, tuff stone interbedded by lava and breccia, and an interlayer of mudstone and calcium sediments; (3) the Ciseuruh Member of the Jampang Formation, which is partly brecciated and overlain by andesite and basalt lava flows; (4) the Ciletuh Formation, mainly composed of sandstone and shale,

*Corresponding author. Email: zhangzhengw@hotmail.com

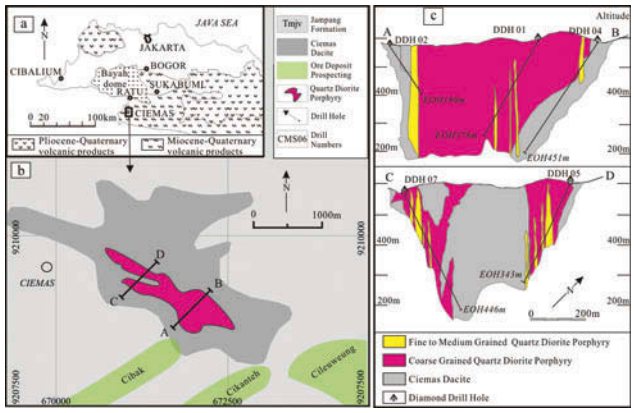

Figure 1. (a) Tectonic sketch map of West Java, Indonesia. (b) Geological sketch map of Ciemas. (c) Section map of the quartz diorite porphyry in Ciemas (modified after Zhang (2010)).

overlain by the Jampang Formation; (5) Ciemas andesite, a widespread rock characterized by abundant coarse-grained quartz phenocrysts; and (6) Quaternary sediments, including some that are widely distributed river terrace gravels and bank sediments.

The regional geology of West Java has been influenced by a NE-trending left-lateral strike-slip fault and the Sumatran right-lateral strike-slip fault, which stretches into West Java (Malod *et al.* 1995). The study area was volcanically active during Mesozoic time, and the fracture structures and distribution of volcanic rock were controlled by the volcanic structure. Intrusions are poorly exposed, and only a quartz diorite porphyry intrusion can be identified on the surface (Figure 1(b) and (c)).

3. Characteristics of quartz diorite porphyry intrusion

The quartz diorite porphyry intrusion is approximately 1000 m long by 500 m wide (Figure 1(b)), intruded into dacite and andesite, and covered by a weathering and alteration zone (Figure 2(a) and (b)). Samples taken by diamond drilling show that the intrusion is mainly composed of coarse-grained quartz diorite porphyry. Some veins of fine- to medium-grained quartz diorite porphyry can be observed surrounding and inside the intrusion (Figure 1(c)).

The quartz diorite porphyry is greyish white (Figure 2 (c) and (f)), but is reddish-brown near its contact due to the ferritization of pyrite (Figure 2(e). The rock has a massive structure and porphyritic texture, with phenocrysts of quartz (Figures 2(b) and 3(c)) and hornblende (Figures 2 (f), 3(a) and (b)) and a matrix composed of cryptocrystalline quartz and feldspar (Figure 3(b) and (c)). Quartz phenocrysts are coarse-grained hexagonal bipyramids (Figure 2(c)), and hornblende phenocrysts are columnar (Figure 2(f) and (b)). Alteration is common in the exposed

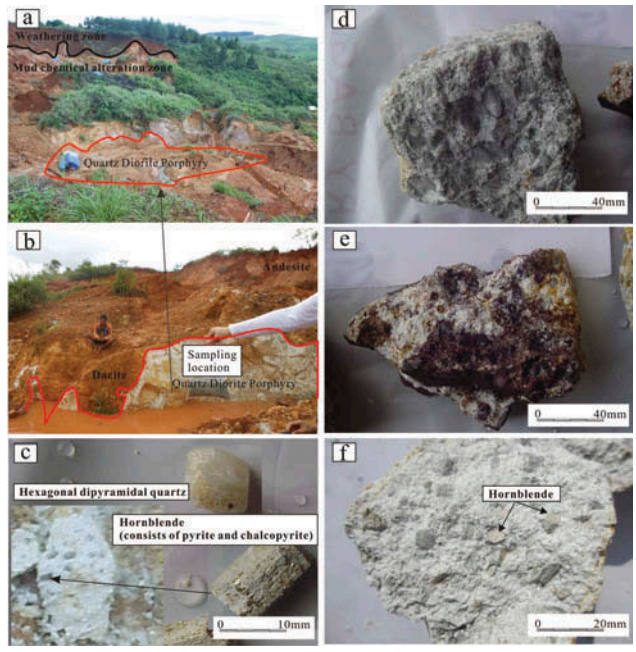

Figure 2. Images of sampling location and samples of quartz diorite porphyry in Ciemas. (a) Exposed quartz diorite porphyry, covered by weathering and alteration zone. (b) Quartz diorite porphyry is greyish white, intruded into andesite and dacite. (c) Samples from diamond drills. Phenocrysts are mainly quartz and hornblende; quartz phenocryst is a coarse-grained hexagonal bipyramid. Disseminated pyrite and chalcopyrite can be seen in the samples. (d) Quartz diorite porphyry is of massive structure and porphyritic texture. (e) Quartz diorite porphyry in the contact zone of intrusion and wall rocks; it is reddish-brown due to ferritization of pyrite. (f) Hornblende phenocryst is columnar.

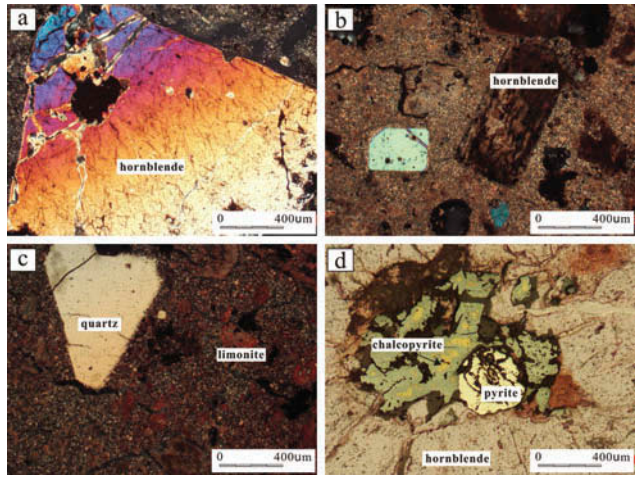

Figure 3. Micrographs of quartz diorite porphyry in Ciemas. (a) Hornblende phenocryst (cross-polarized light). (b) Columnar hornblende phenocryst; the matrix is mainly cryptocrystalline quartz and feldspar with argillization and sericitization alterations (cross-polarized light). (c) Quartz phenocryst; the limonite is due to ferritization of pyrite (cross-polarized light). (d) Pyrite and chalcopyrite in the hornblende phenocryst (reflected light).

rock, with evidence of argillization, silicification, carbonatization, chloritization, epidotization, sericitization (Figure 3(b)), greisenization, etc. Pyritization, sphalerite mineralization, chalcopyritization (Figure 3(d)), and ferritization (Figures 2(e) and 3(c)) can also be seen in the rock.

4. Sampling and analytical methods

Nineteen samples from the quartz diorite porphyry and wall-rock volcanics were collected. Sampling locations and numbers are shown in Figure 4.

All samples were crushed to 200 mesh for whole-rock geochemical analysis, including major, trace, and REE elements. Whole-rock abundances of major elements were analysed by the X-ray fluorescence method at ALS Chemex (Guangzhou) Co., Ltd. (Guangzhou, Guangdong, China). Trace elements and REEs were analysed by inductively coupled plasma mass spectrometry (ICP-MS) at the State Key Laboratory of Ore Deposit Geochemistry, Institute of Geochemistry, Chinese Academy of Sciences. The methods used for all analyses are shown in (Qi *et al.* 2000). The results of major element, trace element, and REE sample composition are shown in Table 1.

U-Pb isotope analyses of zircon were conducted by LA-ICP-MS at the State Key Laboratory of Ore Deposit Geochemistry. The GeoLasPro laser ablation system (Lambda Physik, Gottingen, Germany) and Agilent 7700x ICP-MS (Agilent Technologies, Tokyo, Japan) were used in the analyses. The 193 nm ArF excimer laser, homogenized by a set of beam delivery systems, was focused on zircon surfaces at an energy intensity of 10 J/cm^2. The ablation protocol employed a spot diameter of 32 um at 5 Hz repetition rate for 40 s (equalling 200 pulses). Helium was applied as a carrier gas to efficiently transport aerosol to the ICP-MS. Zircon 91500 was used as an external standard to correct for instrumental mass discrimination and elemental fractionation. Zircon GJ-1 and Plešovice were treated as quality controls for geochronology. Lead abundances of zircon were externally calibrated against NIST SRM 610 with Si as an internal standard, and Zr was used as an internal standard for other trace elements (Liu *et al.* 2010b; Hu *et al.* 2011). Raw data reduction was performed off-line by ICPMSDataCal software (Liu *et al.* 2010a, 2010b). The method used for common lead correction is shown in (Andersen 2002). The concordia diagrams and calculations of weighted average ages were performed by Isoplot/Ex-ver2 (Ludwig 2003). The results of the analyses are shown in Table 2.

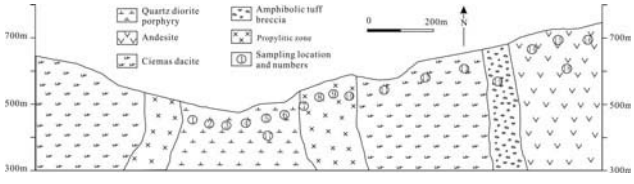

Figure 4. Schematic diagram of sampling the quartz diorite porphyry and wall rocks in Ciemas. (1) CR-1 quartz diorite porphyry; (2) CR-2 quartz diorite porphyry; (3) CR-3 quartz diorite porphyry; (4) CR-4 quartz diorite porphyry; (5) CR-5 quartz diorite porphyry; (6) CR-6 quartz diorite porphyry; (7) CR-7 altered dacite; (8) CR-8 altered dacite; (9) CR-9 altered dacite; (10) CR-10 altered dacite; (11) CR-11 dacite; (12) CR-12 dacite; (13) CR-13 dacite; (14) CR-14 andesite; (15) CR-15 andesite; (16) CR-16 andesite; (17) CR-17 quartz diorite porphyry; (18) CR-18 andesite; and (19) CR-19 amphibolic tuff breccia (zircons for U-Pb dating were selected from samples 17, 18, and 19).

5. Results

5.1. Geochemistry

The quartz diorite porphyry has 63.79–65.44% (average 64.63%) SiO_2, with a high content of Al_2O_3 (16.81–17.92%, average 17.20%) and a low content of MgO (1.01–2.08%, average 1.55%). Total alkalis (Na_2O + K_2O) are 2.64–2.10% and the Rittmann Index σ ($\sigma = (K_2O + Na_2O)^2/(SiO_2–42)$ (Wt%) (Rittmann 1957)) is 0.22–0.46, which shows that the rocks belong to the calc-alkaline-high K calc-alkaline series (Figure 5).

The primitive mantle-normalized trace element patterns of all quartz diorite porphyry samples are similar (Figure 6(a)), showing enrichment in Rb, Th, U, K, La, Ce, Nd, and Sm and depletion of Nb, Ta, Sr, P, Zr, Hf, and Ti. The wall rocks also show similar trace element patterns (Figure 6(b)), which indicates that the intrusion and wall rocks originated from the same magmatic source.

The REE patterns of the quartz diorite porphyry all have enriched LREE and depleted heavy REE (HREE) patterns (Figure 7(a)). The REE contents in the quartz diorite porphyry range from 163 to 247 ppm (average 217 ppm). The ratio ∑LREE/∑HREE ranges from 5.16 to 7.48 (average 6.87). The wall rocks have REE patterns similar to those of quartz diorite porphyry but with much lower overall REE contents (Figure 7(b)). The REE contents in the wall rocks range from 22.6 to 215 ppm (average 111 ppm). The ∑LREE/∑HREE ratio ranges from 2.52 to 22.78 (average 8.02).

Most samples show slightly negative Ce and Eu anomalies (Figure 7). The value of δCe ($\delta Ce = 2*Ce_N/(La_N + Pr_N)$) ranges from 0.69 to 0.92 (average 0.81) and that of δEu ($\delta Eu = 2*Eu_N/(Sm_N + Gd_N)$) from 0.77 to 0.88 (average 0.84) in the quartz diorite porphyry, while δCe ranges from 0.50 to 1.16 (average 0.81) and δEu from 0.52 to 0.97 (average 0.73) in the wall-rock volcanics.

Zircons were separated from the quartz diorite porphyry, andesite, and amphibolic tuff breccia. The zircons are light-coloured, prismatic, and have length:width ratios of 2:1–5:1. Cathodoluminescence (CL) images of the zircons show good crystal morphology and clear oscillatory

Table 1. Major (%), trace, and rare earth ($\times 10^{-6}$) element compositions of magmatic rocks from Ciemas.

Sample	CR-1	CR-2	CR-3	CR-4	CR-5	CR-6	CR-7	CR-8	CR-9	CR-10	CR-11	CR-12	CR-13	CR-14	CR-15	CR-16
SiO_2	64.58	64.99	64.27	64.69	65.44	63.79										
Al_2O_3	17.92	16.84	17.09	17.56	16.81	16.99										
Fe_2O_3	3.68	4.38	4.24	3.82	4.62	5.62										
CaO	0.12	0.13	0.13	0.11	0.1	0.11										
MgO	1.65	2.08	1.7	1.78	1.01	1.1										
Na_2O	0.76	0.55	0.55	0.67	0.33	0.33										
K_2O	1.95	2.09	2.11	2.02	2.76	2.77										
TiO_2	0.59	0.54	0.56	0.57	0.55	0.6										
MnO	0.02	0.03	0.02	0.02	0.02	0.02										
P_2O_5	0.009	0.018	0.016	0.009	0.011	0.015										
LOI	7.58	7.68	7.86	7.68	7.27	7.73										
Total	98.87	99.33	98.55	98.95	98.94	99.09										
Li	10.9	14.1	21.8	10.8	14.3	21.2	23.78	5.41	9.04	2.58	7.08	3.75	5.05	6.38	3.02	2.34
Be	1.38	1.36	1.32	1.26	1.09	1.13	1.49	1.51	1.64	1.26	0.39	0.96	0.83	0.84	0.86	1.18
Sc	13.7	12	12.9	13.1	10.5	11	11.1	10.4	10.8	9.73	6.47	60.1	20.5	21.9	13.6	17.2
V	84	87	90	86	51	51	75.6	119	63.2	79.7	29.9	921	92.3	121	193	115
Cr	24	22	25	24	17	17	28.5	34.7	23.2	36.5	46.5	356	49.1	81.3	30.5	32.6
Co	12.1	15.5	16.5	10.9	15.4	23.9	92.4	109	111	29.5	128	90.9	27	65.6	70.3	94.2
Ni	13.2	15.4	15.6	12.8	12.1	17	14.8	4.72	12.2	13.2	4.55	22	5.21	63.5	6.14	0.9
Cu	5.3	11.2	14.2	5.3	4.8	4.7	49.9	1.12	5.7	4.92	371	187	111	230	4.43	8.75
Zn	30	40	42	38	18	25	65.2	54.1	43.2	76.4	859	540	81.1	42.1	23.5	16.7
Ga	21.4	20.3	20.9	20.4	17.8	19.4	16.9	16.3	15.5	16.9	4.2	14.6	12.5	15.5	13.6	16
Ge	0.19	0.19	0.2	0.19	0.18	0.2	1.36	1.52	1.22	1.31	0.89	0.86	0.95	2	1.34	2.09
As	25.2	20.7	19.2	21.7	54.5	73.9	11.95	10.77	15.27	9.11	118.7	14.93	114.92	7.52	9.45	14.14
Rb	73	77.6	80.7	73.2	97.2	96.7	69.8	59.3	83.8	68.6	24.6	0.67	62.1	3.65	92.1	83.9
Sr	68.3	44	42.4	58	29	29.4	32.3	54.1	25.2	56.2	7.11	3.54	12.6	4.15	23	25.8
Zr	15.1	17.8	18.4	14.5	12.2	14.5	91.3	44.7	105	121	22	267	11.9	66.1	118	112
Nb	5.6	4.8	4.9	5.2	1.9	1.9	6.61	6.76	7.65	5.9	1.56	124	3.31	1.16	7.71	6.03
Mo	1.76	2.77	2.71	1.57	1.35	0.68	2.58	1.01	1.67	1.78	4.72	7.21	2.73	0.56	0.68	1.57
Cd	0.25	0.06	0.07	0.17	<0.02	<0.02	0.56	0.55	0.52	0.56	3.35	0.28	0.42	0.69	0.49	1.35
In	0.047	0.029	0.024	0.045	0.051	0.046	0.08	0.12	0.1	0.08	1.61	0.27	0.31	0.11	0.1	0.29
Sn	13.2	9.8	10.1	11.7	7.4	7.8	12.9	16.4	12.3	11.9	9.92	6.53	8.78	21.7	14.9	43
Sb	0.88	2.66	2.34	0.89	0.9	1.06	5.77	0.32	1.24	0.86	8.48	0.89	16.52	0.43	1.57	0.71
Cs	9.75	10.5	11.1	9.57	7.87	7.42	10.5	3.16	7.3	9.69	1.61	0.2	2.82	0.69	8.1	1.67
Ba	100	80	80	100	200	220	60.1	175	230	97	74.6	16.5	206	30.6	317	310
Hf	0.5	0.6	0.6	0.5	0.5	0.6	2.76	1.48	3.42	3.46	0.65	7.05	0.35	2.13	3.26	3.05
Ta	0.47	0.41	0.42	0.47	0.17	0.18	0.58	0.59	0.67	0.55	0.15	8.36	0.27	0.11	0.7	0.55
W	1.6	1.8	2	1.5	1.1	1.2	381	524	569	130	698	101	136	93.9	277	763
Tl	0.73	0.81	0.83	0.77	0.97	1.02	0.88	0.63	0.92	0.73	0.32	0.04	0.75	0.09	1.09	0.87
Pb	10.1	8.7	8.5	8.2	7.4	9.2	15.5	13.87	9.67	8.87	600.29	23.55	613.12	13.75	9.24	11.89
Bi	0.59	0.9	1.09	0.61	0.89	1.08	1.37	1.31	1.06	0.42	22.8	0.18	5.92	1.9	1.04	2.23
Th	10.4	9.6	10	10.1	9.8	11.1	10.3	12.1	11.2	9.69	2.28	2.12	4.76	0.99	12.3	10.4
U	1.6	1.5	1.8	1.5	1.5	1.8	2.46	1.29	1.86	2.05	0.42	2.61	0.87	0.91	2.04	1.47
La	46.5	51.5	52.8	45.6	34.3	41.2	42.8	10.5	34	43.9	6.41	4.17	49.4	30.6	36.6	3.93

(*Continued*)

Table 1. (Continued).

Sample	CR-1	CR-2	CR-3	CR-4	CR-5	CR-6	CR-7	CR-8	CR-9	CR-10	CR-11	CR-12	CR-13	CR-14	CR-15	CR-16
Ce	91.4	88.9	93	89.9	50.9	66.7	69.4	19.8	45.4	83.4	12.8	10.8	40.7	36	66	7.07
Pr	11.2	11.85	12.25	11.15	8.29	10.1	9.42	2.57	7.57	10.4	1.44	1.1	4.93	6.85	8.17	0.99
Nd	43.1	46	47.7	43.1	33.2	39.8	37.4	10.2	31.4	41.1	5.41	5.17	14.4	29.4	31.2	3.78
Sm	8.6	9.83	9.99	8.71	7.36	8.54	8.26	2.15	6.87	8.26	0.99	1.34	2.37	7.07	6.17	0.9
Eu	2.14	2.77	2.76	2.19	2.18	2.40	2.05	0.44	1.95	2.09	0.21	0.31	0.49	2.22	0.94	0.22
Gd	8.05	9.27	9.43	8.06	7.66	8.69	6.94	1.8	6.8	7.78	0.99	1.35	1.89	6.7	4.44	1.14
Tb	1.16	1.34	1.35	1.19	1.18	1.3	1.19	0.3	1.26	1.24	0.13	0.22	0.25	1.23	0.69	0.23
Dy	6.74	7.69	7.77	7.03	7.21	7.85	6.27	1.73	7.22	6.57	0.61	1.41	1.09	7.03	3.28	1.56
Ho	1.43	1.6	1.62	1.46	1.52	1.67	1.49	0.39	1.65	1.45	0.14	0.32	0.23	1.55	0.68	0.4
Er	3.9	4.38	4.41	4.02	4.12	4.55	4.09	1.17	4.59	3.92	0.4	0.95	0.63	4.09	1.93	1.27
Tm	0.55	0.61	0.61	0.56	0.6	0.66	0.57	0.17	0.68	0.53	0.07	0.18	0.09	0.56	0.25	0.22
Yb	3.32	3.59	3.53	3.41	3.6	4.08	3.57	1.15	4	3.51	0.39	1.38	0.66	3.42	1.66	1.6
Lu	0.48	0.51	0.5	0.48	0.52	0.59	0.53	0.2	0.6	0.53	0.06	0.26	0.09	0.53	0.25	0.27
Y	41.9	47.9	47.9	41.8	45.2	48	44.7	10.8	48.5	41.6	3.43	6.64	4.97	42.4	18.9	11
∑LREE	202.94	210.85	218.50	200.65	136.23	168.74	169.33	45.66	127.19	189.15	27.26	22.89	112.29	112.14	149.08	16.89
∑HREE	25.63	28.99	29.22	26.21	26.41	29.39	24.65	6.91	26.80	25.53	2.79	6.07	4.93	25.11	13.18	6.69
∑REE	228.57	239.84	247.72	226.86	162.64	198.13	193.98	52.57	153.99	214.68	30.05	28.96	117.22	137.25	162.26	23.58
∑L/∑H	7.92	7.27	7.48	7.66	5.16	5.74	6.87	6.61	4.75	7.41	9.77	3.77	22.78	4.47	11.31	2.52
δCe	0.92	0.82	0.83	0.91	0.69	0.75	0.78	0.87	0.64	0.89	0.96	1.16	0.50	0.56	0.87	0.82
δEu	0.77	0.87	0.86	0.79	0.88	0.84	0.81	0.67	0.86	0.79	0.64	0.70	0.69	0.97	0.52	0.66

Note: $\delta Ce = 2*Ce_N/(La_N + Pr_N)$, $\delta Eu = 2*Eu_N/(Sm_N + Gd_N)$, N-normalized to chondrite (Taylor and McLennan 1985); ∑L/∑H = ∑LREE/∑HREE; LOI = loss on ignition.
Sample numbers as in Figure 4.

Table 2. LA- ICP-MS zircon dating results for magmatic rocks in Ciemas.

	Th	U		$^{207}Pb/^{235}U$		$^{206}Pb/^{238}U$		$^{208}Pb/^{232}Th$		$^{207}Pb/^{235}U$		$^{206}Pb/^{238}U$		$^{208}Pb/^{232}Th$	
Analysed point	ppm	ppm	Th/U	Ratio	1σ	Ratio	1σ	Ratio	1σ	Age/Ma	1σ	Age/Ma	1σ	Age/Ma	1σ
CR-17 Quartz diorite porphyry															
CR17-01	277	477	0.58	0.02116	0.00363	0.00264	0.00006	0.00082	0.00003	21.0	4.0	17.0	0.4	16.5	0.6
CR17-02	218	325	0.67	0.02045	0.00307	0.00260	0.00008	0.00081	0.00003	21.0	3.0	16.8	0.5	16.3	0.6
CR17-03	163	505	0.32	0.01767	0.00156	0.00263	0.00005	0.00083	0.00005	18.0	2.0	16.9	0.3	17.0	1.0
CR17-04	185	253	0.73	0.02133	0.00401	0.00234	0.00008	0.00072	0.00003	21.0	4.0	15.1	0.5	14.5	0.5
CR17-05	213	323	0.66	0.02419	0.00319	0.00266	0.00007	0.00081	0.00002	24.0	3.0	17.1	0.5	16.4	0.5
CR17-06	244	594	0.41	0.02064	0.00226	0.00271	0.00006	0.00084	0.00002	21.0	2.0	17.4	0.4	17.1	0.5
CR17-07	378	694	0.55	0.02765	0.00210	0.00280	0.00005	0.00085	0.00002	28.0	2.0	18.0	0.3	17.1	0.3
CR17-08	157	268	0.59	0.02339	0.00379	0.00245	0.00008	0.00075	0.00003	23.0	4.0	15.8	0.5	15.1	0.5
CR17-09	296	459	0.64	0.02431	0.00273	0.00276	0.00006	0.00085	0.00002	24.0	3.0	17.8	0.4	17.1	0.3
CR17-10	145	260	0.56	0.03162	0.00736	0.00262	0.00008	0.00078	0.00004	32.0	7.0	16.9	0.5	15.7	0.9
CR17-11	150	247	0.61	0.02084	0.00732	0.00249	0.00009	0.00077	0.00010	21.0	7.0	16.0	0.6	16.0	2.0
CR17-12	149	425	0.35	0.02183	0.00229	0.00286	0.00007	0.00089	0.00003	22.0	2.0	18.4	0.4	18.0	0.6
CR17-13	110	179	0.61	0.01981	0.00390	0.00257	0.00009	0.00080	0.00005	20.0	4.0	16.5	0.5	16.0	1.0
CR17-14	143	236	0.60	0.01892	0.00303	0.00257	0.00007	0.00080	0.00006	19.0	3.0	16.5	0.5	16.0	1.0
CR17-15	203	382	0.53	0.01868	0.00168	0.00267	0.00005	0.00084	0.00003	19.0	2.0	17.2	0.3	17.0	0.5
CR-18 Andesite															
CR18-01	105	303	0.35	0.02113	0.00292	0.00271	0.00007	0.00084	0.00005	21.0	3.0	17.5	0.4	17.0	0.9
CR18-02	154	364	0.42	0.02050	0.00214	0.00259	0.00006	0.00080	0.00002	21.0	2.0	16.6	0.4	16.2	0.4
CR18-03	199	297	0.67	0.01798	0.00452	0.00283	0.00008	0.00117	0.00029	18.0	5.0	18.2	0.5	24.0	6.0
CR18-04	243	437	0.56	0.02211	0.00267	0.00261	0.00006	0.00080	0.00002	22.0	3.0	16.8	0.4	16.2	0.4
CR18-05	141	350	0.40	0.02072	0.00228	0.00274	0.00006	0.00086	0.00003	21.0	2.0	17.7	0.4	17.3	0.6
CR18-06	303	489	0.62	0.01773	0.00246	0.00265	0.00006	0.00084	0.00006	18.0	2.0	17.1	0.4	17.0	1.0
CR18-07	220	443	0.50	0.02203	0.00527	0.00270	0.00007	0.00084	0.00011	22.0	5.0	17.4	0.4	17.0	2.0
CR18-08	219	511	0.43	0.02062	0.00196	0.00267	0.00005	0.00083	0.00002	21.0	2.0	17.2	0.3	16.8	0.4
CR18-09	441	530	0.83	0.02054	0.00182	0.00266	0.00005	0.00083	0.00002	21.0	2.0	17.1	0.3	16.7	0.3
CR18-10	240	489	0.49	0.02312	0.00248	0.00259	0.00005	0.00079	0.00002	23.0	2.0	16.7	0.4	16.1	0.4
CR18-11	153	401	0.38	0.01755	0.00183	0.00260	0.00005	0.00082	0.00005	18.0	2.0	16.8	0.4	17.0	1.0
CR18-12	129	434	0.30	0.02138	0.00293	0.00264	0.00007	0.00082	0.00005	21.0	3.0	17.0	0.4	16.5	0.9
CR18-13	224	449	0.50	0.02526	0.00220	0.00273	0.00006	0.00083	0.00002	25.0	2.0	17.6	0.4	16.8	0.4
CR18-14	397	575	0.69	0.02835	0.00306	0.00284	0.00006	0.00086	0.00002	28.0	3.0	18.3	0.4	17.3	0.4
CR18-15	196	499	0.39	0.01971	0.00177	0.00280	0.00006	0.00088	0.00004	20.0	2.0	18.0	0.4	17.8	0.7
CR18-16	180	420	0.43	0.02644	0.00243	0.00282	0.00007	0.00086	0.00002	26.0	2.0	18.1	0.4	17.3	0.4
CR18-17	391	697	0.56	0.02152	0.00190	0.00285	0.00005	0.00089	0.00002	22.0	2.0	18.3	0.4	17.9	0.4
CR18-18	135	360	0.38	0.01777	0.00274	0.00269	0.00008	0.00085	0.00011	18.0	3.0	17.3	0.5	17.0	2.0
CR18-19	148	381	0.39	0.01934	0.00227	0.00264	0.00006	0.00083	0.00004	19.0	2.0	17.0	0.4	16.7	0.9
CR18-20	370	641	0.58	0.02425	0.00175	0.00293	0.00006	0.00090	0.00002	24.0	2.0	18.9	0.4	18.3	0.3
CR18-21	270	528	0.51	0.02016	0.00511	0.00276	0.00007	0.00086	0.00012	20.0	5.0	17.8	0.5	17.0	2.0
CR18-22	502	874	0.57	0.02129	0.00088	0.00276	0.00005	0.00078	0.00003	21.4	0.9	17.8	0.3	15.7	0.6
CR18-23	271	581	0.47	0.01825	0.00142	0.00287	0.00006	0.00098	0.00009	18.0	1.0	18.5	0.4	20.0	2.0

(*Continued*)

Table 2. (Continued).

	Th	U		$^{207}Pb/^{235}U$		$^{206}Pb/^{238}U$		$^{208}Pb/^{232}Th$		$^{207}Pb/^{235}U$		$^{206}Pb/^{238}U$		$^{208}Pb/^{232}Th$	
Analysed point	ppm	ppm	Th/U	Ratio	1σ	Ratio	1σ	Ratio	1σ	Age/Ma	1σ	Age/Ma	1σ	Age/Ma	1σ
CR18-24	140	392	0.36	0.01749	0.00232	0.00263	0.00007	0.00083	0.00010	18.0	2.0	16.9	0.4	17.0	2.0
CR18-25	284	578	0.49	0.02160	0.00213	0.00264	0.00005	0.00082	0.00002	22.0	2.0	17.0	0.4	16.5	0.4
CR18-26	155	514	0.30	0.02716	0.00269	0.00289	0.00007	0.00088	0.00002	27.0	3.0	18.6	0.5	17.8	0.5
CR-19 Amphibolic tuff breccia															
CR19-01	220	420	0.52	0.02059	0.00227	0.00253	0.00007	0.00078	0.00002	21.0	2.0	16.3	0.4	15.8	0.4
CR19-02	255	481	0.53	0.01999	0.00194	0.00259	0.00006	0.00081	0.00002	20.0	2.0	16.7	0.4	16.3	0.4
CR19-03	128	255	0.50	0.01770	0.00305	0.00259	0.00008	0.00082	0.00008	18.0	3.0	16.7	0.5	17.0	2.0
CR19-04	291	517	0.56	0.02649	0.00213	0.00279	0.00006	0.00085	0.00002	27.0	2.0	18.0	0.4	17.1	0.4
CR19-05	164	287	0.57	0.02821	0.00376	0.00275	0.00009	0.00083	0.00002	28.0	4.0	17.7	0.6	16.7	0.5
CR19-06	266	396	0.67	0.02514	0.00233	0.00274	0.00007	0.00083	0.00002	25.0	2.0	17.6	0.4	16.9	0.4
CR19-07	216	489	0.44	0.02258	0.00240	0.00275	0.00006	0.00085	0.00002	23.0	2.0	17.7	0.4	17.2	0.4
CR19-08	200	246	0.81	0.01881	0.00417	0.00250	0.00009	0.00078	0.00006	19.0	4.0	16.1	0.6	16.0	1.0
CR19-09	143	253	0.56	0.02808	0.00559	0.00245	0.00009	0.00073	0.00003	28.0	6.0	15.8	0.6	14.8	0.6
CR19-10	214	415	0.52	0.02473	0.00257	0.00252	0.00006	0.00076	0.00002	25.0	3.0	16.2	0.4	15.4	0.4
CR19-11	130	215	0.61	0.02408	0.00514	0.00245	0.00009	0.00074	0.00003	24.0	5.0	15.8	0.6	15.0	0.7
CR19-12	127	243	0.52	0.01725	0.00451	0.00248	0.00009	0.00078	0.00011	17.0	4.0	15.9	0.6	16.0	2.0
CR19-13	131	248	0.53	0.02584	0.00446	0.00262	0.00009	0.00079	0.00003	26.0	4.0	16.9	0.6	16.1	0.6
CR19-14	318	562	0.57	0.02409	0.00211	0.00272	0.00006	0.00083	0.00002	24.0	2.0	17.5	0.4	16.8	0.3
CR19-15	108	195	0.55	0.02918	0.00564	0.00249	0.00009	0.00074	0.00003	29.0	6.0	16.1	0.6	15.0	0.7
CR19-16	160	239	0.67	0.02163	0.00554	0.00238	0.00009	0.00073	0.00004	22.0	6.0	15.3	0.6	14.7	0.8
CR19-17	126	219	0.58	0.01885	0.00369	0.00263	0.00009	0.00083	0.00007	19.0	4.0	16.9	0.6	17.0	1.0
CR19-18	188	354	0.53	0.02324	0.00257	0.00255	0.00006	0.00078	0.00002	23.0	3.0	16.4	0.4	15.8	0.4
CR19-19	140	305	0.46	0.03360	0.00890	0.00256	0.00010	0.00075	0.00004	34.0	9.0	16.5	0.6	15.2	0.8
CR19-20	128	472	0.27	0.02370	0.00256	0.00271	0.00006	0.00083	0.00002	24.0	3.0	17.5	0.4	16.8	0.5
CR19-21	106	433	0.24	0.02252	0.00284	0.00271	0.00006	0.00084	0.00004	23.0	3.0	17.4	0.4	16.9	0.7

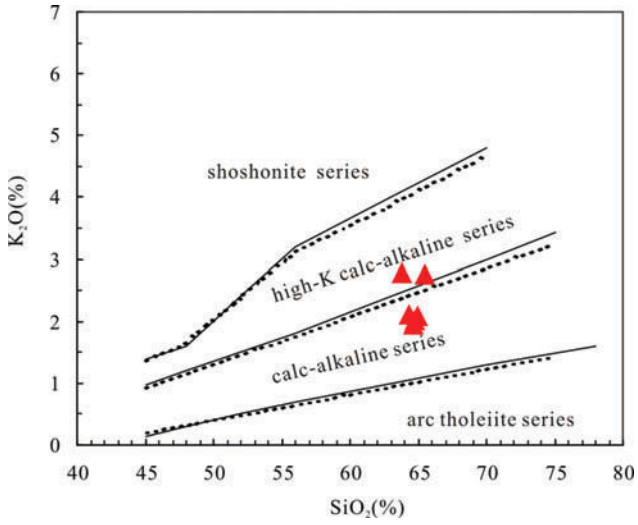

Figure 5. Diagram of SiO_2-K_2O of quartz diorite porphyry in Ciemas (the solid line is according to Peccerillo and Taylor (1976) and the dotted line is according to Middlemost (1985)).

zoning (Figure 8), typical for magmatic zircons. The Th/U of zircons ranges from 0.32 to 0.73 (average 0.56) in quartz diorite porphyry, from 0.30 to 0.83 (average 0.48) in andesite, and from 0.24 to 0.81 (average 0.53) in amphibolic tuff breccia.

In the zircon U-Pb $^{206}Pb/^{238}U$-$^{207}Pb/^{235}U$ concordia diagram, the analysed data fall near concordia. The $^{207}Pb/^{235}U$ ratios show a broad range because of the

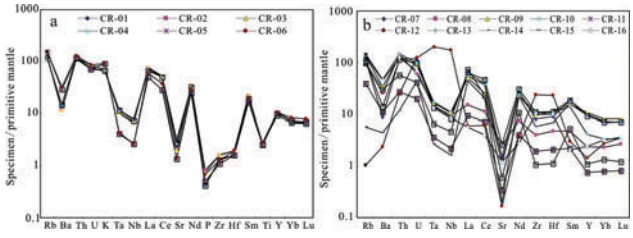

Figure 6. Spider diagrams of trace elements normalized to the primitive mantle (Sun and McDonough 1989). (a) Quartz diorite porphyry; (b) wall rock. Sample numbers as in Figure 4.

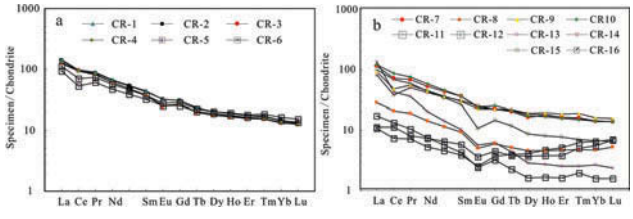

Figure 7. REE patterns of chondrite samples (Taylor and McLennan 1985). (a) Quartz diorite porphyry; (b) wall rock. Sample numbers as in Figure 4.

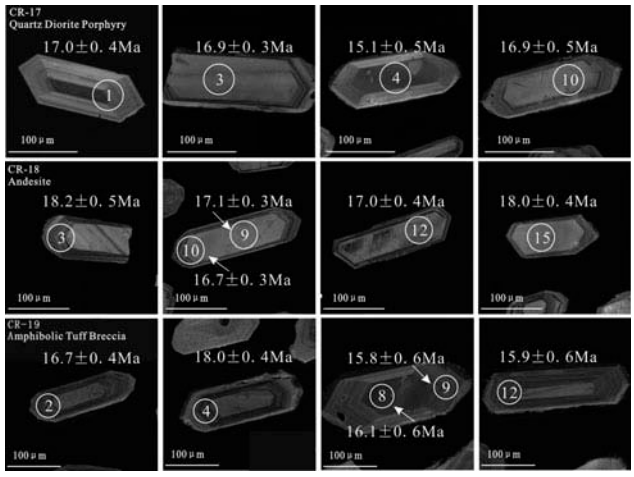

Figure 8. CL images of representative zircons analysed for *in situ* U-Pb of quartz diorite porphyry, andesite, and amphibolic tuff breccia in Ciemas.

young ages of zircons and the low precision of ^{207}Pb content measurement. However, because $^{206}Pb/^{238}U$ ages are consistent, the weighted average $^{206}Pb/^{238}U$ is most reliable (Compston *et al.* 1992). The calculated $^{206}Pb/^{238}U$ age of the andesite is 17.5 ± 0.3 Ma (MSWD = 2.6, n = 26) (Figure 9(a)), that of the amphibolic tuff breccia is 16.9 ± 0.3 Ma (MSWD = 2.5, n = 21) (Figure 9(b)), and that of quartz diorite porphyry is 17.1 ± 0.4 Ma (MSWD = 3.8, n = 15) (Figure 9(c)). All three age ranges calculated are within the range of experimental error, implying that the rocks all formed at approximately the same time during the early Miocene.

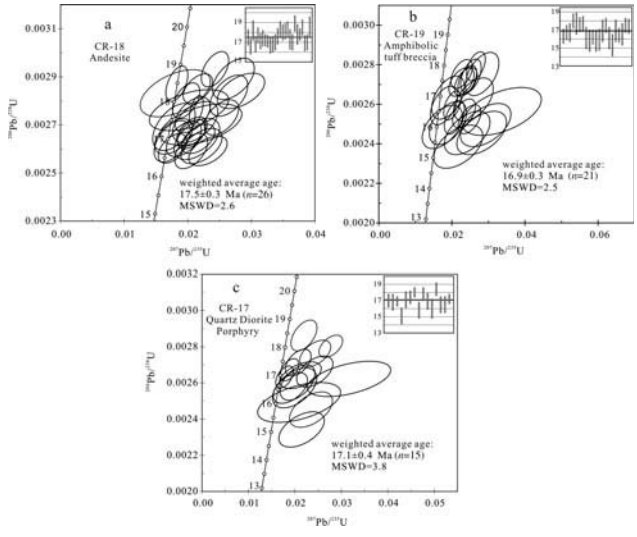

Figure 9. Zircon U-Pb concordia diagram of andesite (a), amphibolic tuff breccia (b), and quartz diorite porphyry (c) in Ciemas.

6. Discussion

6.1. Ages of emplacement of porphyry

Java is part of the Indonesian islands and is located in the south of Sundaland on the Eurasian Plate. Sundaland is the core of mainland Southeast Asia (Bemmelen 1949) and was formed by epicontinental accretion in the Late Cretaceous. The basement contains granite and metamorphic rocks formed in the Palaeozoic and the Mesozoic (Audley-Charles *et al.* 1988; Metcalfe 1996). In the Late Cretaceous, a block from Gondwanaland accreted to the east of Java and the west of Sulawesi (Smyth *et al.* 2007). From the Late Cretaceous to the Palaeocene, most of Sundaland was exposed continent, and the south of Java may have been a passive continental margin. A subduction zone formed southwest of Sulawesi with the subduction of the Indian–Australian Plate beneath the Eurasian Plate. The Sunda volcanic arc formed along the northern margin of this active convergence and has been active since at least the Eocene (Katili 1975; Hamilton 1979).

Based on K-Ar dating results, Soeria-Atmadja *et al.* (1994) proposed that volcanism in Java can be divided into three magmatic belt formation events: late Eocene to early Miocene (40–19–18 Ma), late Miocene to Pliocene (12 or 11–2 Ma), and Quaternary. The late Eocene to early Miocene belt was emplaced along the southern part of Java, trending from west to east. The late Miocene to Pliocene belt occurred further north, parallel to the older belt and in places is overlain by Quaternary volcanics. However, evidence of magmatism between 18 and 12 Ma is lacking in Java, which Soeria-Atmadja *et al.* (1994) attributed to the relative movement of the plates after a major collision in the early Miocene. This collision was thought to have resulted also in the northward shift of the magmatic arc.

Our new data close some of the Miocene magmatic gap in Java. LA-ICP-MS U-Pb zircon ages of the andesite, amphibolic tuff breccia, and quartz diorite porphyry are 17.5 ± 0.3, 16.9 ± 0.3, and 17.1 ± 0.4 Ma, respectively. The ages of andesite and amphibolic tuff breccia represents the time of volcanism, while that of quartz diorite porphyry represents the time of intrusion. The calculated ages indicate that the intrusion and wall rocks have a consistent diagenetic age and were probably all formed by mid-Miocene magmatism, which would have been part of the late Eocene to early Miocene magmatic belt that formed in southern Java.

6.2. Petrogenesis

Enrichment of the large-ion lithophile elements (LILEs) K, Rb, Th, and U and depletion of the high-field strength elements (HFSEs) Nb, Ta, Zr, Hf, and P are the major geochemical characteristic of arc magmatic rocks (Kay 1980; Perfit *et al*. 1980; McCulloch and Gamble 1991; Hawkesworth *et al.* 1997). It is generally accepted that the addition of fluid from the dehydration of subducted slab resulted in partial melting of overlying mantle wedge (Morris *et al.* 1990; Sigmarsson *et al.* 1990; Plank and Langmuir 1993). Comparing the composition of sediments in the subduction zone to that of magma indicates that the enrichment of LILE arc magmatic rocks stems from the addition of sediments from the oceanic crust (Plank and Langmuir 1993).

From south to north, magmatic rocks of the three aforementioned belts belong to the low-K tholeiitic, high-K or tephrite, and ultrapotassic series (Soeria-Atmadja *et al.* 1994). Incompatible elements apparently increase with each subsequent magmatic belt formation and within each of these magmatic events. This increase may be attributed to either changes in composition of the subducted materials or the progressive enrichment of incompatible elements in the mantle wedge as a consequence of the long period of subduction (Soeria-Atmadja *et al.* 1994).

The quartz diorite porphyry belongs to the calc-alkaline-high K calc-alkaline series and is enriched in K compared with other magmatic rocks in southern Java. This may be due to the older age of the quartz diorite porphyry, as the compositions of younger magmas belong to the high-K or tephrite series.

The primitive mantle-normalized trace element patterns of quartz diorite porphyry and wall rocks are similar, with relative enrichments in the LILEs Rb, Th, and U and relative depletions of the HFSEs Nb, Ta, Zr, and Hf. The trace element patterns normalized to the primitive mantle are similar to those of the typical arc magmatic rocks. However, the abundance of Rb, Sr, and Ba in wall-rock volcanics is lower than that in quartz diorite porphyry and is highly variable. This may be attributed to the alteration in wall rocks, resulting in the loss of some trace elements. REE patterns of quartz diorite porphyry and wall rocks are similar, with enriched LREEs, depleted HREEs, and negative Eu anomaly. This is similar to the patterns of typical arc dacite (Martin 1999). The $(La/Yb)_N$ ratios of quartz diorite porphyry and wall rock are in the range 1.66–14.9 (average 7.13) and 6.44–10.1 (average 8.59, except for CR-13), respectively, which are close to those of arc dacite and granodiorite (7.5 and 6.6, respectively) (Martin 1999). The negative Eu anomaly (average δEu of quartz diorite porphyry and wall rocks is 0.81 and 0.73, respectively) and depletion of Sr is associated with the fractional crystallization of plagioclase. High Y contents (average for quartz diorite porphyry and wall rocks is 45.5 and 23.3 ppm, respectively) and high Yb contents (average for quartz diorite porphyry and wall rocks is 3.59 and 2.13 ppm, respectively) clearly distinguish these from adakites ($Y \leq 18$ ppm and Yb ≤1.9 ppm), which originate from the partial melting of young (<25 Ma) subducted oceanic crust (Defant and Drummond 1990; Martin 1999).

Cr and Ni contents in quartz diorite porphyry are in the ranges 17–25 ppm (average 21.5 ppm) and 12.1–17 ppm

(average 14.4 ppm), respectively, which are similar to those of typical arc granodiorite (average Cr and Ni 23 and 10 ppm, respectively) (Martin 1999). However, average Cr and Ni contents in wall rocks are 40.2 (except for CR-12) and 14.7, respectively, both higher than that in the quartz diorite porphyry. The contents of Co and V in wall rocks are also higher than that in quartz diorite porphyry.

The geochemical characteristics of the intrusion and wall rocks indicate that both originated from the same arc magmatism event. As the Indian–Australian Plate subducted beneath the Eurasian Plate, the addition of fluid from dehydration of the subducted slab resulted in partial melting of the overlying mantle wedge and generated mafic magma. This evolved further in the crust, resulting in early Miocene arc magmatism in the Ciemas area. Here, andesite and dacite lavas were erupted and simultaneously intruded by mineralized quartz diorite porphyry formed by the intrusion of differentiated arc magma.

7. Conclusion

The intrusion into Ciemas andesite and dacite can be defined as quartz diorite porphyry by its petrographic and petrologic characteristics. The quartz diorite porphyry belongs to the felsic calc-alkaline-high K calc-alkaline series and has geochemical characteristics similar to those of the volcanic wall rocks, which are enriched in the LILEs Rb, Th, and U and depleted in the HFSEs Nb, Ta, Zr, and Hf. The REE patterns are LREE-enriched, with negative Eu anomalies as is typically the case for felsic arc magmatic rocks.

LA-ICP-MS U-Pb zircon ages of wall rock andesite, amphibolic tuff breccia, and quartz diorite porphyry are 17.5 ± 0.3, 16.9 ± 0.3, and 17.1 ± 0.4 Ma, respectively, which indicates that the intrusion and wall rocks were all formed by the same mid-Miocene magmatic event. Formation of the volcanic andesite and dacite and the intrusion of differentiated arc magma that formed the quartz diorite porphyry were related to the northward subduction of the Indian–Australian Plate. The addition of fluid from the dehydration of the subducted slab resulted in the partial melting of the overlying mantle wedge, ultimately resulting in formation of the arc magmatic rocks.

Funding

The research is financially supported by the Natural Science Foundation of China [NFSC Number 913282009 and 41173064] and the 12th Five-Year Plan project of State Key Laboratory of Ore-deposit Geochemistry, Chinese Academy of Sciences [SKLODG-ZY125-08].

References

Andersen, T., 2002, Correction of common lead in U–Pb analyses that do not report ^{204}Pb: Chemical Geology, v. 192, p. 59–79. doi:10.1016/S0009-2541(02)00195-X

Audley-Charles, M., Ballantyne, P., and Hall, R., 1988, Mesozoic-Cenozoic rift-drift sequence of Asian fragments from Gondwanaland: Tectonophysics, v. 155, p. 317–330. doi:10.1016/0040-1951(88)90272-7

Bemmelen, R.W., 1949, The geology of Indonesia: The Hague, Martinus Nijhoff.

Bemmelen, R.W., 1970, The geology of Indonesia (second edition): The Hague, Martinus Nijhoff.

Compston, W., Williams, I., Kirschvink, J., Zichao, Z., and Guogan, M., 1992, Zircon U-Pb ages for the early Cambrian time-scale: Journal of the Geological Society, v. 149, p. 171–184. doi:10.1144/gsjgs.149.2.0171

Defant, M.J., and Drummond, M.S., 1990, Derivation of some modern arc magmas by melting of young subducted lithosphere: Nature, v. 347, p. 662–665. doi:10.1038/347662a0

Hamilton, W.B., 1979, Tectonics of the Indonesian region: Geological Survey Professional Paper 1078: Washington, DC, U.S. Government Printing Office.

Hawkesworth, C., Turner, S., McDermott, F., Peate, D., and Van Calsteren, P., 1997, U-Th isotopes in arc magmas: Implications for element transfer from the subducted crust: Science, v. 276, p. 551–555. doi:10.1126/science.276.5312.551

Hu, Z.C., Liu, Y.S., Chen, L., Zhou, L., Li, M., Zong, K.Q., Zhu, L.Y., and Gao, S., 2011, Contrasting matrix induced elemental fractionation in NIST SRM and rock glasses during laser ablation ICP-MS analysis at high spatial resolution: Journal of Analytical Atomic Spectrometry, v. 26, p. 425–430. doi:10.1039/c0ja00145g

Katili, J.A., 1975, Volcanism and plate tectonics in the Indonesian island arcs: Tectonophysics, v. 26, p. 165–188. doi:10.1016/0040-1951(75)90088-8

Kay, R.W., 1980, Volcanic arc magmas: Implications of a melting-mixing model for element recycling in the crust-upper mantle system: The Journal of Geology, v. 88, p. 497–522. doi:10.1086/628541

Liu, Y.S., Gao, S., Hu, Z.C., Gao, C.G., Zong, K.Q., and Wang, D.B., 2010a, Continental and oceanic crust recycling-induced melt–peridotite interactions in the Trans-North China Orogen: U–Pb dating, Hf isotopes and trace elements in zircons from mantle xenoliths: Journal of Petrology, v. 51, p. 537–571. doi:10.1093/petrology/egp082

Liu, Y.S., Hu, Z.C., Zong, K.Q., Gao, C.G., Gao, S., Xu, J., and Chen, H.H., 2010b, Reappraisement and refinement of zircon U-Pb isotope and trace element analyses by LA-ICP-MS: Chinese Science Bulletin, v. 55, p. 1535–1546. doi:10.1007/s11434-010-3052-4

Ludwig, K.R. 2003, User's manual for Isoplot 3.00: A geochronological toolkit for Excel: Berkeley, CA, Berkeley Geochronology Center Special Publication, v. 4, 67 p.

Malod, J., Karta, K., Beslier, M., and Zen, M., 1995, From normal to oblique subduction: Tectonic relationships between Java and Sumatra: Journal of Southeast Asian Earth Sciences, v. 12, p. 85–93.

Marcoux, E., and Milési, J.-P., 1994, Epithermal gold deposits in West Java, Indonesia: Geology, age and crustal source: Journal of Geochemical Exploration, v. 50, p. 393–408. doi:10.1016/0375-6742(94)90033-7

Martin, H., 1999, Adakitic magmas: Modern analogues of Archaean granitoids: Lithos, v. 46, p. 411–429. doi:10.1016/S0024-4937(98)00076-0

McCulloch, M.T., and Gamble, J., 1991, Geochemical and geodynamical constraints on subduction zone magmatism: Earth and Planetary Science Letters, v. 102, p. 358–374. doi:10.1016/0012-821X(91)90029-H

Metcalfe, I., 1996, Gondwanaland dispersion, Asian accretion and evolution of eastern Tethys: Australian Journal of Earth Sciences, v. 43, p. 605–623. doi:10.1080/08120099608728282

Middlemost, E., 1985, Magmas and magmatic rocks: London, Longman, p. 1–266.

Morris, J., Leeman, W., and Tera, F., 1990, The subducted component in island arc lavas: Constraints from Be isotopes and B–Be systematics: Nature, v. 344, p. 31–36.

Nicholls, I., Whitford, D., Harris, K., and Taylor, S., 1980, Variation in the geochemistry of mantle sources for tholeiitic and calc-alkaline mafic magmas, Western Sunda volcanic arc, Indonesia: Chemical Geology, v. 30, p. 177–199. doi:10.1016/0009-2541(80)90105-9

Peccerillo, A., and Taylor, S.R., 1976, Geochemistry of Eocene calc-alkaline volcanic rocks from the Kastamonu area, Northern Turkey: Contributions to Mineralogy and Petrology, v. 58, p. 63–81. doi:10.1007/BF00384745

Perfit, M., Gust, D., Bence, A.E., Arculus, R., and Taylor, S., 1980, Chemical characteristics of island-arc basalts: Implications for mantle sources: Chemical Geology, v. 30, p. 227–256. doi:10.1016/0009-2541(80)90107-2

Plank, T., and Langmuir, C.H., 1993, Tracing trace elements from sediment input to volcanic output at subduction zones: Nature, v. 362, p. 739–743. doi:10.1038/362739a0

Qi, L., Hu, J., and Gregoire, D.C., 2000, Determination of trace elements in granites by inductively coupled plasma mass spectrometry: Talanta, v. 51, p. 507–513.

Rittmann, A., 1957, On the serial character of igneous rocks: Egyptian Journal of Geology, v. 1, p. 23–48.

Sigmarsson, O., Condomines, M., Morris, J., and Harmon, R., 1990, Uranium and ^{10}Be enrichments by fluids in Andean arc magmas: Nature, v. 346, p. 163–165.

Smyth, H., Hamilton, P., Hall, R., and Kinny, P., 2007, The deep crust beneath island arcs: Inherited zircons reveal a Gondwana continental fragment beneath East Java, Indonesia: Earth and Planetary Science Letters, v. 258, p. 269–282. doi:10.1016/j.epsl.2007.03.044

Soeria-Atmadja, R., Maury, R., Bellon, H., Pringgoprawiro, H., Polve, M., and Priadi, B., 1994, Tertiary magmatic belts in Java: Journal of Southeast Asian Earth Sciences, v. 9, p. 13–27. doi:10.1016/0743-9547(94)90062-0

Sun, S.S., and McDonough, W.F., 1989, Chemical and isotopic systematics of oceanic basalts: Implications for mantle composition and processes: Geological Society, London, Special Publications, v. 42, p. 313–345. doi:10.1144/GSL.SP.1989.042.01.19

Taylor, S.R., and McLennan, S.M., 1985, The continental crust: Its composition and evolution: Oxford, Blackwell.

Whitford, D., Nicholls, I., and Taylor, S., 1979, Spatial variations in the geochemistry of Quaternary lavas across the Sunda arc in Java and Bali: Contributions to Mineralogy and Petrology, v. 70, p. 341–356. doi:10.1007/BF00375361

Zhang, Z.W., 2010, Geological evaluation report of Ciemas Gold Orefield in Indonesia (in Chinese), p. 1–42 (in press).